Electrochemistry Communications 13 (2011) 818–821

Contents lists available at ScienceDirect

Electrochemistry Communications

journal homepage: www.elsevier.com/locate/elecom

# Ex-situ depth-sensing indentation measurements of electrochemically produced Si–Li alloy films

Benjamin Hertzberg, Jim Benson, Gleb Yushin *

*School of Materials Science and Engineering, Georgia Institute of Technology, Atlanta, GA, 30332, USA*

ARTICLE INFO

*Article history:*
Received 19 April 2011
Received in revised form 10 May 2011
Accepted 11 May 2011
Available online 18 May 2011

*Keywords:*
Anode
Alloy
Lithium
Silicon
Modulus
Hardness

ABSTRACT

We report for the first time ex-situ measurements of the Young's modulus and hardness of Si and Si–Li alloy thin film electrodes at various stages of lithium insertion *via* depth-sensing indentation experiments. Lithium is electrochemically inserted into the Si electrode, after which its mechanical properties are investigated in an anoxic environment. The Young's modulus was found to decrease from an initial value of 92 GPa for pure Si to 12 GPa at full lithium insertion ($Li_{15}Si_4$). The hardness changes from an initial value of 5 GPa for Si to 1.5 GPa for $Li_{15}Si_4$.



## 1. Introduction

Silicon (Si) anodes have been the subject of extensive investigation in the last years [1–14]. The challenges of maintaining the integrity of Si electrodes due to the dramatic expansion of the material during Li insertion remain the major obstacle [6]. In a recent study Si placed in a confined space was found to mechanically deform during Li insertion [7]. When Si nanoparticle anodes are produced with rigid binders [8,11,12], one may expect that a similar type of deformation may take place during the expansion of the particles into the differently shaped electrode pores. The endurance of the Si-binder interface, critical for stable anode operation, must exceed the amplitude of the interfacial stresses caused by the initial expansion of Si particles, which are, in turn, dependent on the plasticity and elastic modulus of lithiated Si. Unfortunately, little experimental data are available on the mechanical properties of Si lithiated to various degrees. Such information is, however, crucial for the design and successful implementation of stable Si-based anodes.

By using density functional theory (DFT) Shenoy et al. calculated the Young's modulus and Poisson ratios of both amorphous and crystalline Li–Si phases at a range of different concentrations [13]. Interestingly, for Li fraction changes from 0.5 to 0.76 (LiSi to $Li_{13}Si_4$) the modulus was found to exhibit minimal changes [13]. Using electrochemical strain microscopy Kalinin et al. were able to directly map the lithiation/delithiation process with a nanometer-level resolution [14]. In the initial charging process, the grain boundaries were observed to become heavily lithiated first; subsequently, the lithiated areas expanded inward into the higher-density areas as the anode approached full lithiation [14]. Sethuraman et al. proposed a novel method to perform in-situ measurements of the stress in thin Si–Li alloy film during lithiation and delithiation by monitoring changes in the curvature of substrate using a multi-beam optical sensor [15]. While the authors concluded that the biaxial modulus could be approximated by the rule of mixtures, they observed rather small changes in the modulus when Li fraction changes in the range from 0.3 to 0.75 [15,16].

In this study, we employed depth-sensing indentation (nanoindentation) measurements to acquire direct ex-situ experimental values of the Young's modulus and hardness of nanocrystalline Si films at various stages of lithiation. The obtained results suggest some deviation in the Young's modulus from the predictions of a simple rule of mixing, which agrees with the actual data collected in prior theoretical and experimental studies [13,15], but disagrees with the simplified conclusions of their authors.

## 2. Experimental methods

In order to avoid substrate effects in our nanoindentation measurements, a thick (~6 μm) Si film was used in our experiments. Si film was deposited using chemical vapor deposition (CVD) at 750 °C. Silane ($SiH_4$) diluted to 5 wt.% with Ar was selected as the precursor gas. The deposition was performed at a low-pressure (~1 Torr) to achieve high coating uniformity [7,9]. Carbon-coated nickel foils with a total thickness of ~120 um were used as substrates

* Corresponding author. Tel. +1 4043853261.
*E-mail address:* yushin@gatech.edu (G. Yushin).

1388-2481/$ – see front matter © 2011 Elsevier B.V. All rights reserved.
doi:10.1016/j.elecom.2011.05.011

for Si deposition and as current collectors for electrochemical measurements.

For electrochemical Li insertion experiments, Si film-coated Ni foil electrodes were assembled into 2016 lithium-ion coin cells inside an Ar filled glovebox. 1 M lithium hexafluorophosphate ($LiPF_6$) salt, dissolved in ethylene, dimethyl, and diethyl carbonate (1:1:1 wt. % solution), was used as an electrolyte. Li foil (electrochemical grade, Alfa Aesar) of 1 mm in thickness was used as a counter electrode. Li insertions into Si films were performed in a series of two steps. First, a constant current was applied at a slow C/40 rate until the potential reached a pre-selected value. This was followed by a constant potential step, at which the selected potential was applied to the cell until the current dropped to 1–5% of the C/40 current applied during the constant current step.

To prepare samples for mechanical measurements, the lithiated Si electrodes were removed from the coin cell in an Ar box and mounted on a stainless steel substrate using a thermoplastic polymer adhesive. Great care was taken in order to avoid a reaction of lithiated Si with air or moisture during the time between cell disassembly and depth-sensing indentation measurements inside a nanoindenter chamber filled with Ar. After mounting on a rigid stainless steel substrate, the samples were dipped into an anhydrous dimethyl carbonate (DMC) filled vial, placed inside a double-walled Ar-filled container and sealed. Before indentation, ultra high purity Ar (99.9999%, Air Gas) was purging the sealed indentation chamber at 0.5 scfm for 15 min and continued for the duration of the experiments. During the short (~10 s) transfer of the samples from the container to the Ar-filled nanoindenter chamber, the samples were coated with an ~1 mm layer of DMC, which evaporated in the chamber in about 30 min during a continuous Ar purge.

Depth-sensing indentation measurements were performed on a Hysitron TI 900 TriboIndenter. A diamond cube corner tip (Northstar, radius <40 nm) was used for the measurements. Calibration was performed using a polycarbonate standard with Young's modulus 3.1 GPa and a hardness of 200 MPa, and a 6 coefficient fitting curve. Indentations were done using max loads of 6000–8500 μN. The loading and unloading rates ranged from 300 to 350 μN/s and were the same for loading and unloading. 16 indentations were made in each sample using the same experimental parameters and spaced 10 μm apart. The average values for the modulus and hardness are reported.

Reduced modulus values were calculated from the unloading curve using the methods developed by Oliver and Pharr [17]. Area was determined by calibration of the tip geometry as a function of penetration depth. Stiffness measurements were made by fitting the unloading of an indent to a power law function using a regression analysis. This allows the slope at the initial unloading to be calculated analytically and reduces the dependence of the method on the amount of creep occurring in the samples. The hardness was calculated using the calibrated area function and the maximum load of the indent. While localized stresses produced during nanoindentation may create concentration gradients and local variations in mechanical properties [18], these effects were not considered in our calculations.

## 3. Results and discussion

Fig. 1a shows the cross-sectional micrograph of the deposited Si film. The films' thicknesses obtained from SEM were in a good agreement with what was obtained from the mass changes observed in the sample after CVD deposition, assuming the density of the deposited Si to be 2.3 g/cm$^3$. XRD confirmed the formation of nanostructured Si. In contrast to Si CVD deposited at 500 °C, which showed XRD-amorphous microstructure [7,9], the deposition performed for the current studies at 750 °C revealed distinct Si peak formation. Fig. 1b shows a typical high-resolution portion of the XRD pattern for the as-deposited unlithiated Si thin film. The broad Si peak visible at 28.7 corresponds to diffraction from the {111} family of planes. Using an instrumental standard and the Scherrer method, the average grain size was calculated as 74 nm.

Fig. 2a shows an example of the galvanostatic Li insertion profile for the produced Si film anodes. The shape of the profile is similar to the profiles previously reported in literature for other Si electrodes (see e.g. Refs. [3,9,15]). In contrast to intercalation-type electrode materials, these profiles do not exhibit horizontal plateaus and cover a larger potential range. The following constant potentials were selected for the electrochemical alloying: 0.174 V (for LiSi), 0.137 V (for $Li_{1.68}Si$), 0.078 V (for $Li_{2.61}Si$) and 0.010 V (for $Li_{3.75}Si$). Due to the large Si film thickness and high Si capacity, Li losses due to SEI formation (no more than 1%, estimated) were neglected in our calculations of the alloys' composition.

Examples of typical load vs. displacement curves for nanoindentations on lithium-silicon thin films are presented in Fig. 2b. These graphs show the load-unload behavior for pure Si films and for Si films lithiated to different final compositions. We can see the progressive transformation of the material as more lithium is inserted. At the same value of the applied load the nanoindenter tip penetrates to larger depth for higher Li content, indicating a systematic reduction in hardness upon Li insertion into Li–Si alloy. The slope of the unloading curve also decreases with increasing degree of lithiation, indicating a reduction in Young's modulus. Occasionally, an “elbow” in the unloading curves of lithiated samples (Fig. 2c) was observed. In pure Si this feature is associated with pressure induced crystalline-to-amorphous phase transformations [19]. If this is also true for Li–Si alloys, then this observation suggests the presence of nanocrystalline grains in all the lithiated films.

Fig. 2d shows the load vs. displacement curves for the $Li_{1.08}Si$ sample. While some variation in the loading curves is observed, the slopes of the unloading curves are commonly very similar, indicating high degree of homogeneity of the Young's modulus throughout the

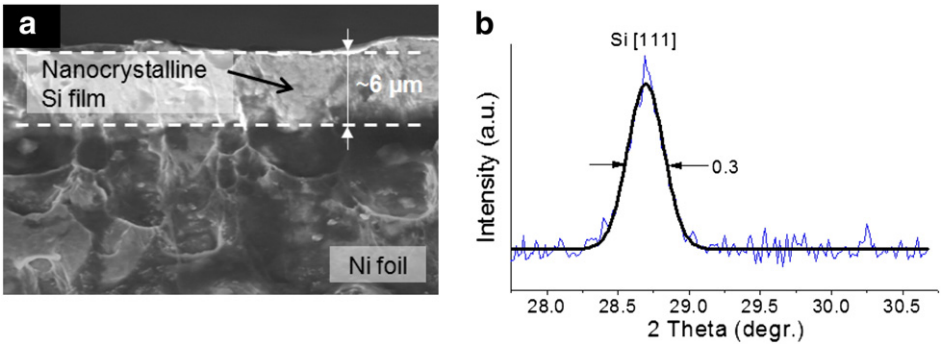


**Fig. 1.** (a) Cross-sectional SEM micrograph of a CVD-deposited Si film on C-coated Ni foil substrate, (b) high-resolution X-ray diffraction pattern of the Si film.

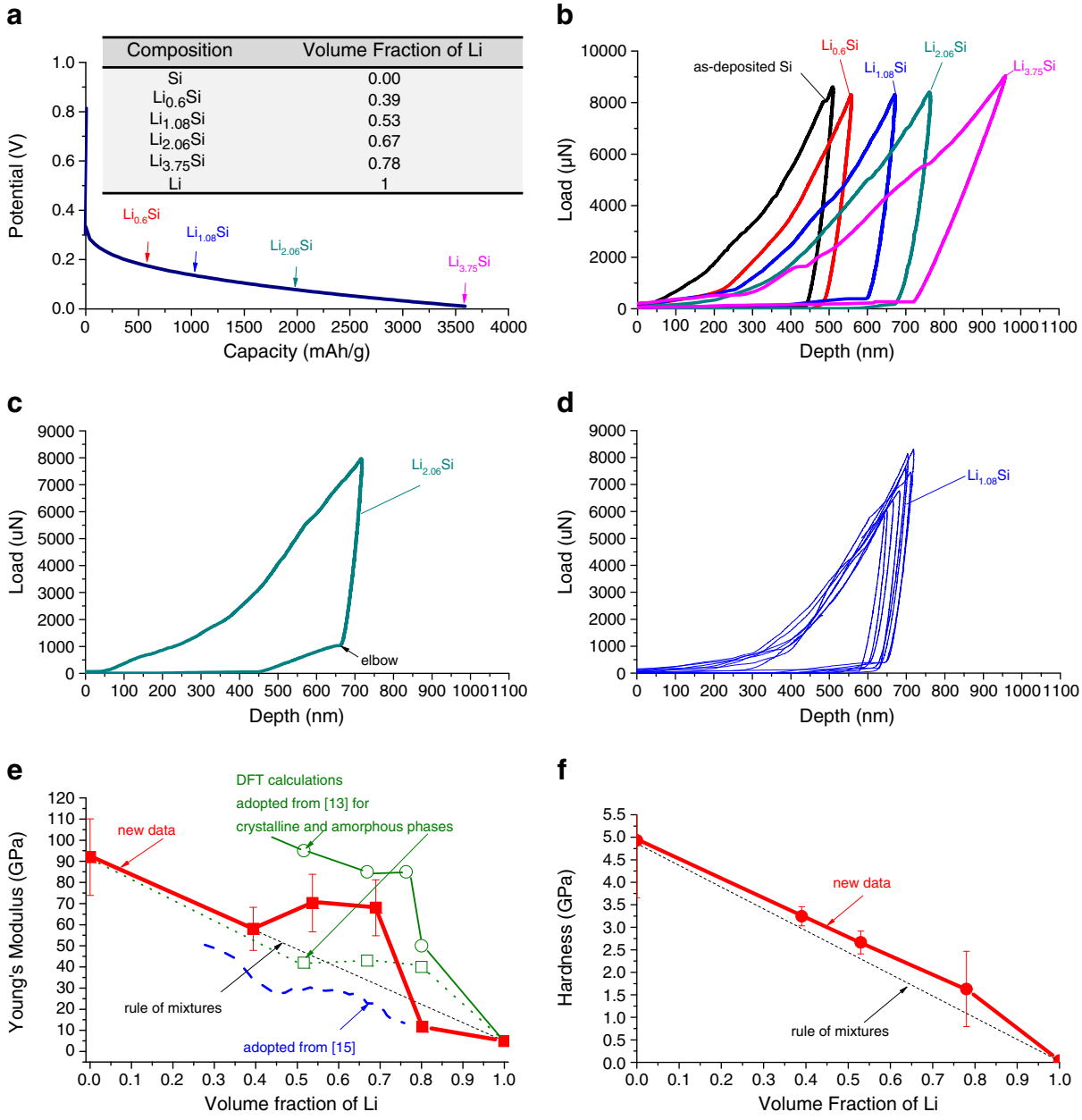


**Fig. 2.** (a) Electrochemical profile for lithium insertion into nanocrystalline Si film; (b) load-displacement curves for Si film samples at various stages of lithiation; (c) a load-displacement curve with an "elbow" in the unloading curve; (d) load-displacement curves for Si film lithiated to $Li_{1.08}Si$; (e) Young's modulus of Li–Si alloys as function of volume fraction of Li; (f) hardness of Li–Si alloys as function of volume fraction of Li.

sample. The slopes of the unloading curves were used to determine the average Young's modulus of our samples. Fig. 2e shows the changes in the Young's modulus as a function of the volume fraction of lithium in the film, calculated assuming theoretical values for the density and molar mass of Li and Si. For comparison purposes, we have also included a theoretical measurement of the Young's modulus based on a linear rule of mixtures:

$$E = E_{Li}V_{Li} + E_{Si}V_{Si}$$

where $V_{Li}$ and $V_{Si}$ are the volume fractions of Li and Si, respectively, in the film, and $E_{Li}$ and $E_{Si}$ are the experimentally determined modulus of microcrystalline Li and nanocrystalline Si films, respectively. Note that the atomic and volume fractions are very similar (<4% difference).

The Young's modulus of nanocrystalline Si film measured from the load-unload curves was found to be 92 GPa, close to the values reported for amorphous (90 GPa) silicon [13]. The Young's modulus of Li was determined to be 5 GPa, consistent with the reported values [15]. Our experiments show when the thin film is lithiated to $Li_{0.6}Si$, the Young's modulus decreases linearly to a value of 58 GPa, as would be predicted by the rule of mixtures. Interestingly, however, higher degree of lithiation to ~$Li_{1.08}Si$ and $Li_{2.06}Si$ leads to the increase in the Young's modulus. A similar increase was also observed in Ref. [15], although the absolute values of the Young's modulus are higher in our measurements. Specifically, in this range the Young's modulus remains constant at ~70 GPa, significantly exceeding the linear rule of mixtures. This value, however, is an average between the DFT-predicted Young's modulus for amorphous and crystalline phases of similar compositions [13]. The value of the Young's modulus is related to the average stiffness of inter-atomic bonds. However, the charge state of individual atoms, the ionic character and stiffness of individual Si–Li bonds (and to a smaller degree, the stiffness of Si–Si and Li–Li bonds) as

well as the number of such bonds should strongly depend not only on the Li fraction but also on the position of a particular atom and its surroundings [13]. Therefore, the observed deviations from the rule of mixtures are believed to be reasonable even for nanocrystalline or amorphous films. Another interesting observation was the steep decrease in Young's modulus from ~70 GPa to ~12 GPa for samples lithiated to a maximum level ($Li_{3.75}Si$ or $Li_{15}Si_4$). A somewhat similar (yet, smaller in magnitude) decrease was predicted for crystalline phase but not for amorphous one [13]. Such a sharp decrease in Young's modulus could be related to the formation of Li-rich areas in the grain boundary regions within the sample [14], which may control the overall elastic properties of the sample. It is also possible that vacancies or microvoids could form within the film after the Li insertion when the film partially transforms from amorphous $Li_{3.75}Si$ to the more thermodynamically stable (nano)crystalline $Li_{15}Si_4$ phase, which would also decrease the Young's modulus.

Changes in the hardness of the nanocrystalline Si film upon lithiation, as estimated from the load vs. displacement curves, were observed to exhibit few features (Fig. 2f). The hardness varies linearly with the volume fraction of Li in the film. The fully lithiated film remains considerably harder than Li metal and retains about 30% of the hardness of the as-deposited Si.

## 4. Conclusion

We report depth-sensing indentation measurements of electrochemically lithiated Si films. The load vs. displacement curves for nanoindentations on Li–Si thin films showed gradually decreasing hardness. The changes in Young's modulus from ~90 GPa for as-deposited Si to ~12 GPa for samples lithiated to a maximum level showed a relatively good agreement with DFT calculations and recent experimental studies. For Li volume fraction up to ~0.375 the Young's modulus agrees well with a linear rule of mixtures. For Li–Si alloys with Li fraction in the range of 0.52–0.67 the Young's modulus remains constant at ~70 GPa. However, increasing the Li content to the maximum level of 0.78 results in a sharp decrease in Young's modulus.

## References

[1] H. Kim, J. Cho, Nano Lett. 8 (2008) 3688.
[2] C.K. Chan, H.L. Peng, G. Liu, K. McIlwrath, X.F. Zhang, R.A. Huggins, Y. Cui, Nat. Nanotechnol. 3 (2008) 31.
[3] S.D. Beattie, D. Larcher, M. Morcrette, B. Simon, J.M. Tarascon, J. Electrochem. Soc. 155 (2008) A158.
[4] M.N. Obrovac, L.J. Krause, J. Electrochem. Soc. 154 (2007) A103.
[5] H. Kim, B. Han, J. Choo, J. Cho, Angew. Chem. Int. Ed. 47 (2008) 10151.
[6] R. Chandrasekaran, A. Magasinski, G. Yushin, T.F. Fuller, J. Electrochem. Soc. 157 (2010) A1139.
[7] B. Hertzberg, A. Alexeev, G. Yushin, J. Am. Chem. Soc. 132 (2010) 8548.
[8] A. Magasinki, B. Zdyrko, I. Kovalenko, B. Hertzberg, I. Burtovyy, T. Fuller, I. Luzinov, G. Yushin, ACS Appl. Mater. Interfaces 2 (2010) 3004.
[9] A. Magasinski, P. Dixon, B. Hertzberg, A. Kvit, J. Ayala, G. Yushin, Nat. Mater. 9 (2010) 353.
[10] U. Kasavajjula, A.J. Appleby, J Power Sources 163 (2007) 1003–1039.
[11] J.S. Bridel, T. Azais, M. Morcrette, J.M. Tarascon, D. Larcher, Chem. Mater. 22 (2010) 1229.
[12] J. Li, R.B. Lewis, J.R. Dahn, Electrochem. Solid State Lett. 10 (2007) A17.
[13] V.B. Shenoy, P. Johari, Y. Qi, J Power Sources 195 (2010) 6825.
[14] N. Balke, S. Jesse, Y. Kim, L. Adamczyk, A. Tselev, I.N. Ivanov, N.J. Dudney, S.V. Kalinin, Nano Lett. 10 (2010) 3420.
[15] V.A. Sethuraman, M.J. Chon, M. Shimshak, N. Van Winkle, P.R. Guduru, Electrochem. Comm. 12 (2010) 1614.
[16] V.A. Sethuraman, M. Shimshak, V. Srinivasan, P.R. Guduru, J. Power Sources 195 (2010) 5062.
[17] W. Oliver, G.M. Pharr, J. Mater. Research 7 (1992) 1564.
[18] V.A. Sethuraman, A.F. Bower, P.R. Guduru, J. Electrochem. Soc. 157 (2010) 1253.
[19] V. Domnich, Y. Gogotsi, S. Dub, Appl. Phys. Lett. 76 (2000) 2214.